Design and characterization of a spatially distributed multibeam field emission x-ray source for stationary digital breast tomosynthesis

Xin Qian[a)]
Department of Physics and Astronomy, University of North Carolina at Chapel Hill, Chapel Hill, North Carolina 27599

Ramya Rajaram and Xiomara Calderon-Colon
Curriculum in Applied Sciences and Engineering, University of North Carolina at Chapel Hill, Chapel Hill, North Carolina 27599

Guang Yang
Department of Physics and Astronomy, University of North Carolina at Chapel Hill, Chapel Hill, North Carolina 27599

Tuyen Phan
Department of Biomedical Engineering, University of North Carolina at Chapel Hill, Chapel Hill, North Carolina 27599

David S. Lalush
Department of Biomedical Engineering, University of North Carolina at Chapel Hill, Chapel Hill, North Carolina 27599 and Department of Biomedical Engineering, North Carolina State University, Raleigh, North Carolina 27659

Jianping Lu
Department of Physics and Astronomy, University of North Carolina at Chapel Hill, Chapel Hill, North Carolina 27599 and Curriculum in Applied Sciences and Engineering, University of North Carolina at Chapel Hill, Chapel Hill, North Carolina 27599

Otto Zhou[b)]
Department of Physics and Astronomy, University of North Carolina at Chapel Hill, Chapel Hill, North Carolina 27599; Curriculum in Applied Sciences and Engineering, University of North Carolina at Chapel Hill, Chapel Hill, North Carolina 27599; and Lineberger Comprehensive Cancer Center, University of North Carolina at Chapel Hill, Chapel Hill, North Carolina 27599

(Received 27 May 2009; revised 6 August 2009; accepted for publication 7 August 2009; published 4 September 2009)

Digital breast tomosynthesis (DBT) is a limited angle computed tomography technique that can distinguish tumors from its overlying breast tissues and has potentials for detection of cancers at a smaller size and earlier stage. Current prototype DBT scanners are based on the regular full-field digital mammography systems and require partial isocentric motion of an x-ray tube over certain angular range to record the projection views. This prolongs the scanning time and, in turn, degrades the imaging quality due to motion blur. To mitigate the above limitations, the concept of a stationary DBT (s-DBT) scanner has been recently proposed based on the newly developed spatially distributed multibeam field emission x-ray (MBFEX) source technique using the carbon nanotube. The purpose of this article is to evaluate the performance of the 25-beam MBFEX source array that has been designed and fabricated for the s-DBT system. The s-DBT system records all the projection images by electronically activating the multiple x-ray beams from different viewing angles without any mechanical motion. The configuration of the MBFEX source is close to the published values from the Siemens Mammomat system. The key issues including the x-ray flux, focal spot size, spatial resolution, scanning time, beam-to-beam consistency, and reliability are evaluated using the standard procedures. In this article, the authors describe the design and performance of a distributed x-ray source array specifically designed for the s-DBT system. They evaluate the emission current, current variation, lifetime, and focal spot sizes of the source array. An emission current of up to 18 mA was obtained at 0.5×0.3 mm effective focal spot size. The experimentally measured focal spot sizes are comparable to that of a typical commercial mammography tube without motion blurring. Trade-off between the system spatial resolution, x-ray flux, and scanning time are also discussed. Projection images of a breast phantom were collected using the x-ray source array from 25 different viewing angles without motion. These preliminary results demonstrate the feasibility of the proposed s-DBT scanner. The technology has the potential to increase the resolution and reduce the imaging time for DBT. With the present design of 25 views, they demonstrated

experimentally the feasibility of achieving 11 s scanning time at full detector resolution with 0.5 $\times$0.3 mm source resolution without motion blur. The flexibility in configuration of the x-ray source array will also allow system designers to consider imaging geometries that are difficult to achieve with the conventional single-source rotating approach. © *2009 American Association of Physicists in Medicine*. [DOI: 10.1118/1.3213520]

Key words: tomosynthesis, breast imaging, x-ray, carbon nanotube, field emission

I. INTRODUCTION

Mammography is currently the most effective screening and diagnostic tool for early detection of breast cancer. It has been attributed as a major factor in reducing breast cancer mortality rate in recent years.[1,2] However, the current two-view mammography method lacks sensitivity and has a very high false alarm rate. X-ray digital breast tomosynthesis (DBT) is an emerging limited angle computed tomography (CT) technique for producing multislice images to provide depth resolution and improved contrast. It has the potential to allow radiologists to detect tumors at an early stage even in very dense breasts using a similar dose as the common two-view mammography.[3–5] Currently, several DBT scanners from commercial vendors are under clinical trial.

The designs of all current DBT scanners are based on a full-field digital mammography system.[5–10] To generate the limited angle series of projection images, a mammography x-ray tube moves along an arc above the partially compressed breast. The scanners by Siemens and Hologic operate in a continuous motion mode. The x-ray tube moves continuously across an arc, while x-ray beam is switched on for a short period of time when the tube reaches the viewing position and the detector is in the acquisition window. The motion of the x-ray source during the finite exposure time smears the object and degrades the system resolution.[10] The reported scan time of the Siemens system is 20 s for 25 views and 39 s for 49 views for a total exposure of 80–144 m As.[11] The focal spot blurring during each exposure is estimated to be ~0.7 mm for a full resolution scan of 25 views in 20 s and more than 1 mm when the scanning time is shortened to 13 s; this blurring is significantly larger than the intrinsic focal spot size (FSS) (~0.3 mm) of the mammography x-ray tube.[12] Although the Hologic scanner uses less projection views and has a shorter scanning time compared to the Siemens model, similar amount of motion-induced blurring has also been observed.[10] The GE system operates in the step-and-shoot mode where source comes to a complete stop at each position before x-ray exposure. The system mechanical instability from acceleration and deceleration of the source limits the speed by which the tube can be moved from view to view.[13] The imaging quality of all current DBT scanners is also compromised by the patient motion during the relatively long scanning time.[14] The linear motion of the x-ray source makes it difficult to explore other imaging geometries that require a nonlinear arrangement of the x-ray viewing points.[15] The already long scanning time prevents further optimization of the x-ray energy spectrum which has the potential to increase the image contrast but requires a significantly higher x-ray output power in order to maintain a comparable imaging time.[16–19]

In the current design, the scanning speed and the focal spot blurring are interconnected. To minimize the patient motion, the scanning speed should be as high as the detector frame rate allows. However, higher scanning speed means that the x-ray tube travels a larger distance during the finite x-ray exposure time window. This problem can, in principle, be mitigated by using a shorter x-ray pulse width, which requires a higher x-ray tube power to maintain the same imaging dose. Due to constraints from the anode heat load, there is, however, limited room for increasing the x-ray power with the current rotating anode mammography x-ray tubes without sacrificing the x-ray focal spot size.

One way to overcome this limitation is to use either multiple individual x-ray tubes or a source with a scanning x-ray beam. This concept has been investigated in the past. The dynamic spatial reconstructor uses a large number of x-ray tubes mounted on a CT gantry to collect project images at high temporal resolution.[20] The system achieved one of the first high resolution cardiac CT images. The design is, however, not practical for clinical use because of issues including cost and size. A dual-source CT scanner has recently been introduced commercially for high resolution and dual energy CT imaging.[21] The electron-beam CT (Ref. 22) and the scanning beam digital x-ray (SBDX)[23,24] utilize an electromagnetic field to steer the electron beam to different spots on the x-ray target to produce a scanning x-ray beam without mechanical motion. Such sources are large and, in the case of SBDX, have limited angular range.

We have recently demonstrated a multibeam field emission x-ray (MBFEX) technology using the carbon nanotube (CNT) field emitters.[25,26] The spatially distributed MBFEX source can generate x-ray radiation from multiple viewing angles by electronically activating the corresponding CNT field emission cathodes. Activation of the x-ray beams can be carried out either sequentially to generate a scanning x-ray beam or in parallel based on a preprogramed multiplexing scheme.[27,28] The technology enables the design of tomography systems with great flexibility in source configuration and imaging sequence. It is now being actively investigated for both preclinical[29] and clinical[30] imaging applications. Based on this MBFEX technology, we recently proposed the concept of a *stationary* DBT (s-DBT) scanner.[31] The proposed system generates all the projection images by electronically activating the multiple x-ray beams from different viewing angles without any mechanical motion. It has the potential to reduce the imaging time, increase the resolution, and sim-

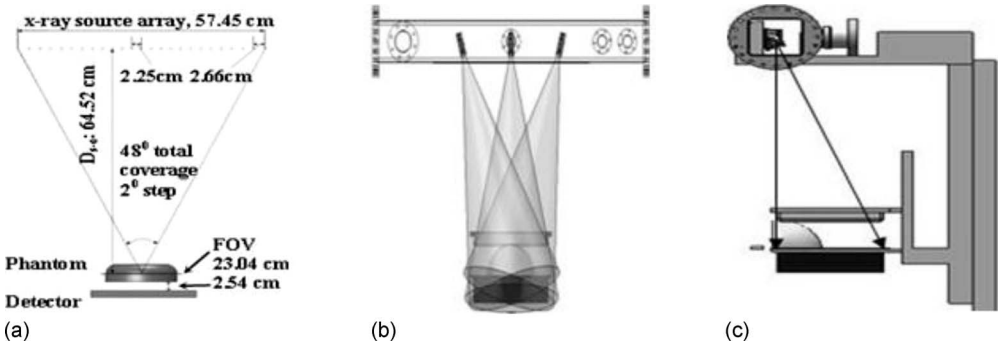

FIG. 1. (a) The geometry of the s-DBT scanner with the MBFEX source which has 25 x-ray beams placed in a linear array parallel to the detector plane. (b) The orientation of the individual x-ray source assembly with respect to the object. (c) The side view from CAD drawings of the s-DBT scanner shows the positions of the source, the detector, and the compression pad. X-ray anodes are positioned above the edge of the detector.

plify the system design. Here, we report a detailed study on the design and the performance characteristics of a MBFEX source designed specifically for s-DBT. The source comprises of 25 individually controllable x-ray beams that operate at 30 keV and cover 48° angular range. Key issues including the x-ray flux, spatial resolution, scanning time, beam-to-beam consistency, and reliability are evaluated.

II. METHOD

II.A. MBFEX source design and construction

Because of the flexibility in configuring the distributed source, several geometrical parameters need to be considered in designing the s-DBT system and MBFEX source. The first is the arrangement of the multiple x-ray beams with respect to the object position and the detector plane. In the current DBT scanners, the x-ray tube moves along an arc above the compressed breast with the exposure points evenly distributed along the rotation route. The MBFEX source technology allows the individual x-ray beams to be arranged in any arbitrary pattern, for example, along a line or on a two-dimensional matrix. In the current study, the multiple x-ray beams are positioned in a straight line parallel to the detector plane for simplicity in design and manufacturing, as illustrated in Fig. 1(a). The second set of parameters is the number of views, their angular coverage, and the distances between the object, the detector, and the source. Here, the MBFEX source is designed to have 25 x-ray beams spanning a distance of 57 cm from end to end. At a source-object distance (SOD) of 64 cm, it provides 48° coverage. The linear spacing between the x-ray beams varies to provide an even 2° angular spacing. The object is placed on a stage with a 2.54 cm air gap between the detector and the object. These parameters are chosen to be close to the published values from the Siemens Mammomat systems.[11]

The 25 individual x-ray generating units ("beams") are housed inside a custom-made stainless steel vacuum chamber with 25 corresponding x-ray windows. The x-ray anodes are tilted toward the center of the object (defined as the isocenter). The centers of the focal points remain on a straight line that is parallel to the detector plane, as illustrated in Fig. 1(b). Each x-ray window is covered by a 30 μm thick Mo foil which provides the vacuum seal and also serves as the x-ray filter. The size of the x-ray exit window is 1 cm in diameter to collimate the x-ray beam to cover only the detector surface, as illustrated in Fig. 1(c).

Each x-ray generating unit comprises of a CNT field emission cathode, a gate electrode to extract the electrons, and a modified Einzel-type electrostatic lens[32] to focus the field emitted electrons to a small area on a Mo anode, as shown in Fig. 2. The anode, focusing electrodes 1 and 2, and the gate electrode are electrically connected to the corre-

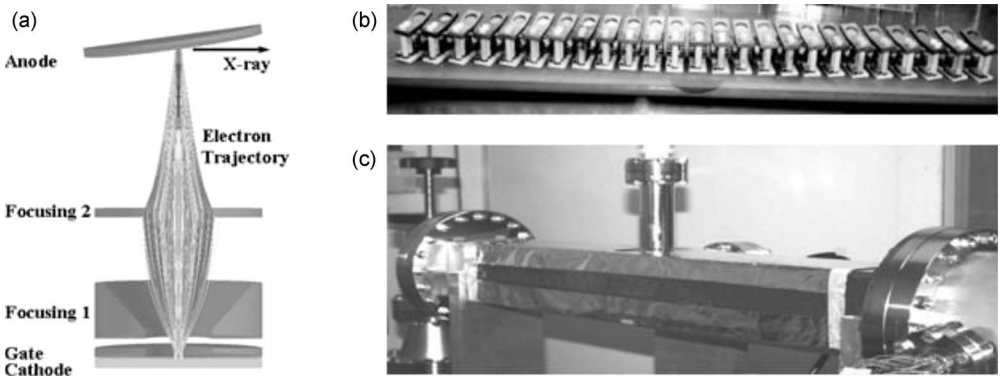

FIG. 2. (a) A schematic showing one x-ray pixel with a modified Einzel lens and the trajectory of the field emitted electron beam. (b) A photo of the 25 x-ray beams assembled on a base plate before electrical connection. (c) A photo of the custom-made x-ray chamber.

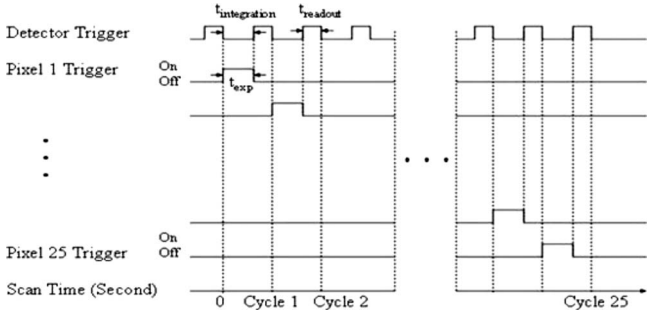

FIG. 3. Timing diagram for the 25-source tomosynthesis system. t_{exp} is the exposure time of x-ray sources, $t_{exp} \leq t_{integration}$. 5 V is used as the trigger voltage to turn on and off the MOSFET.

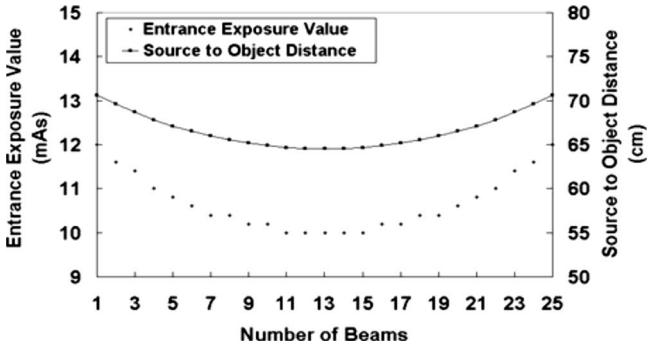

FIG. 5. The design values of the SODs for the different x-ray beams and the calculated exposure value needed from each beam to maintain the constant entrance exposure at the object, assuming that the central beam is 10 m As.

sponding electrodes on the adjacent x-ray generating units. They are connected, respectively, to the following four power supplies: Matsusada AU-40P30 (40 kV, 30 mA), Matsusada AU-5R20 (5 kV, 20 mA), Stanford Research PS350 (2.5 kV, 10 mA), and Keithley 248 (5 kV, 5 mA). The CNT cathodes are connected to the metal-oxide-semiconductor field-effect transistor (MOSFET) switching circuit described below. A vacuum pump is connected to the side flange on the tube to provide 10^{-7}–10^{-8} Torr base pressure. Figure 2 shows the 25 x-ray units assembled on a base plate without the electrical connections.

A flat panel detector (Varian Medical System, Salt Lake City, Utah, Paxscan 2520) is used for imaging acquisition. With a 127 μm pixel pitch, the total array size is 1536 $\times$1920. The detector readout time $t_{readout}$ is 0.128 s without binning and 0.032 s with 2×2 binning. The maximum frame rate is 3.75 frames/s at full resolution and 7.5 frames/s with 2×2 binning.

II.B. Control electronics and interface

The source operates in a sequential mode where the x-ray beam from each x-ray source is activated sequentially by switching on and off the connection to the CNT cathodes. This is accomplished through a MOSFET based control unit we have described previously.[31] In brief, the drain, gate, and source legs of the MOSFET are connected to the cathode, the transistor-transistor logic (TTL) trigger signal provided by the field-programable gate array (FPGA) card (NI PCI-7830R), and a common ground, respectively. When the TTL trigger signal is at low state, the conduction channel between the source and the drain legs is closed and no electron is emitted from the CNT cathode and no x-ray radiation is generated. When the TTL trigger signal is at high state, the cathode is grounded and electrons are extracted by the electrical field applied between the gate electrode and the cathode, and x-ray radiation is produced. The 25 x-ray sources can be switched individually at any given time during the imaging acquisition. The timing of the 25-source tomosynthesis system is shown in Fig. 3. During one normal scan, the FPGA card sends a pulse waveform to the gate of MOSFET simultaneously. The digital pulse of *i*th source's waveform is synchronized to *i*th camera exposure time. Variable resistors are added for compensation of the variations in the individual cathode performance. One limitation of this design is that the breakdown voltage of the MOSFET used is 1500 V, which limits the highest electrical field can be applied to the gate electrode. To minimize the current fluctuation and decay and to reduce source to source variation, an electrical compensation loop is also incorporated to automatically adjust the gate voltage to maintain a constant preset emission current.

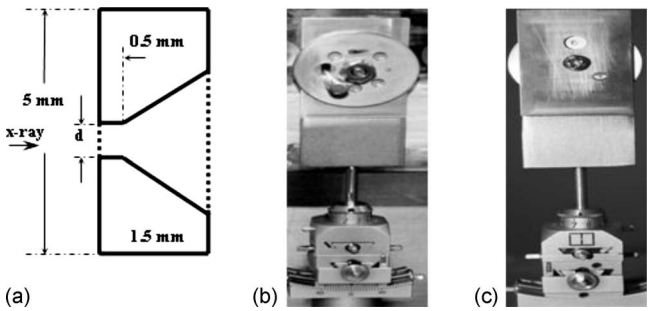

FIG. 4. (a) Cross section of the pinhole phantom, (b) back side of the wheel unit, this side faces detector, and (c) front side of the wheel unit, this side faces x-ray tube.

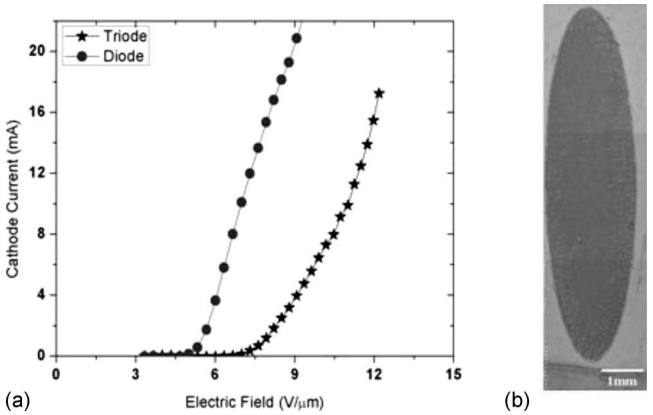

FIG. 6. (a) The emission current versus gate voltage collected using a 2 $\times$8 mm elliptical cathode in the diode and triode modes. (b) Scanning electron microscope image of the elliptical CNT cathode.

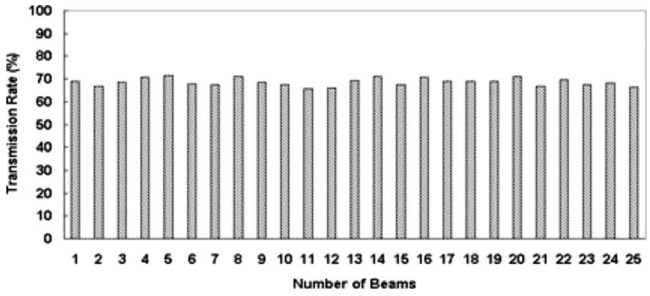

FIG. 7. Transmission rate for all 25 x-ray beams is around 70%. The variation is 1.36%.

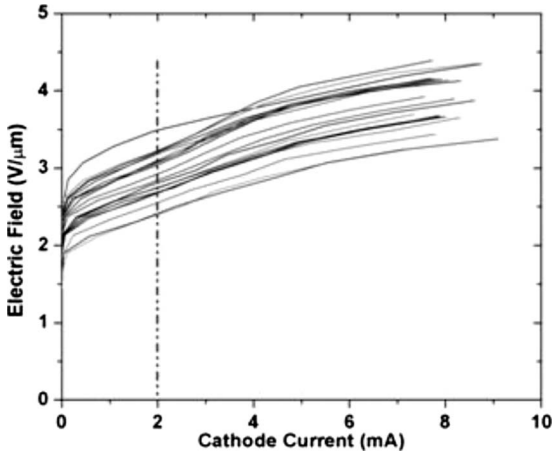

FIG. 9. Field emission characteristics of the CNT cathode measured in the diode mode. The measurement conditions are 10 ms pulse and 1 Hz.

II.C. CNT field emission cathode

To evaluate the x-ray tube current and focal spot size that can be achieved with this design, CNT cathodes with different dimensions were fabricated using the electrophoretic deposition method developed in our laboratory.[33] The emission currents that can be extracted from different size CNT cathodes were evaluated first in the diode mode and then in the actual x-ray tube assembly with the extraction and focusing electrodes. In the diode mode the intrinsic properties were measured in parallel-plate geometry where the CNT film was the cathode and a metal plate the anode. In the x-ray source assembly, the performance was tested by measuring the emission current as a function of the gate electrical field, while the voltages applied to the focusing electrodes and the anode were held constant. The leakage currents to the gate and two focusing electrodes were also recorded at every applied voltage, from which the x-ray tube current (the anode current) was computed.

II.D. X-ray focal spot size measurement

The effective x-ray focal spot sizes for the individual x-ray beams were measured following the European standards (EN 12543-2) (Ref. 34) using a gold-platinum pinhole (Ogussa, Inc., Vienna, Austria). The diameter of the pinhole is $d=100\pm5$ μm with 500 μm length and 12° opening angle, as illustrated in Fig. 4(a). The pinhole phantom was fitted into a stainless steel wheel which has four holes with respective diameters of 3, 1, 5, and 5 mm. The pinhole phantom was put into the 5 mm hole. The wheel was combined with a stainless steel plate to block the rest of the x-ray except the beam going through the pinholes. The whole unit was put on a goniometer mounted on a translation stage for ease of alignment, as shown in Figs. 4(b) and 4(c). Alignment of the pinhole with the x-ray focal spot was aided by a laboratory laser.

After alignment, the electrical potentials applied to the two focusing electrodes were adjusted to optimize the electron focusing optics. The gate voltage (V_g) and anode voltage (V_a) were set at 800 V and 28 kVp, respectively. The measurement was carried out for all 25 x-ray beams. Source-to-

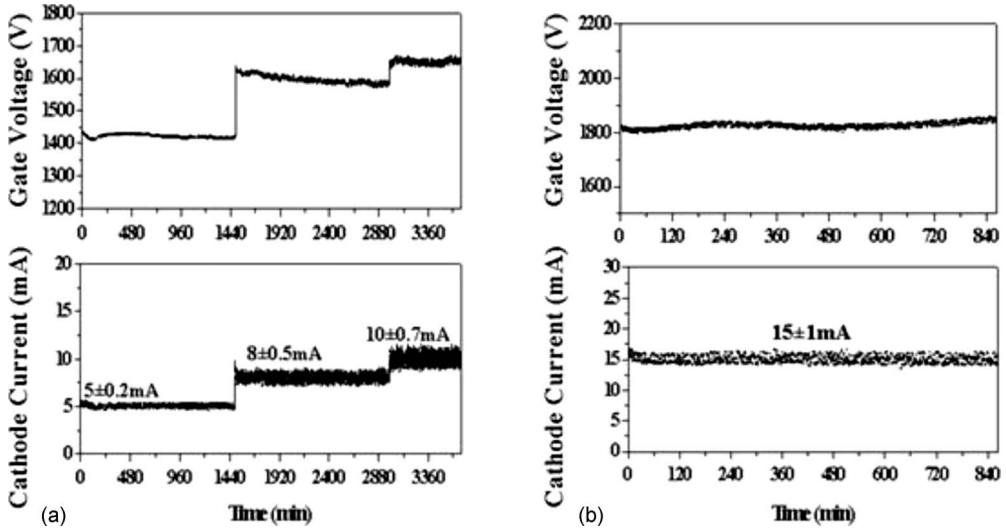

FIG. 8. Electron field emission current from a 2×8 mm elliptical CNT cathode measured in the triode mode. The applied gate voltage was varied to hold the emission current constant. The measurement conditions are (a) 1 s pulse width, 0.2, 0.125, and 0.15 Hz at 5, 8, and 10 mA, respectively. (b) 10 ms pulse width, 1 Hz.

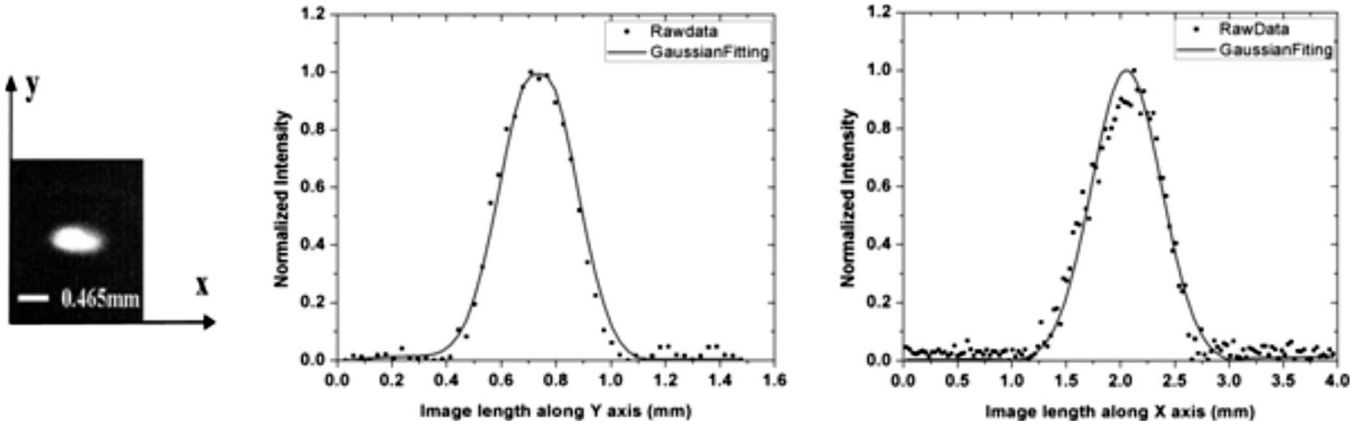

FIG. 10. The projection image of the focal spot of 3 mm diameter circular cathode; Gaussian fitting curves for intensity profiles along the *y* and *x* axes. The scale bar in the projection image and the image length units in Gaussian fits images have been normalized using the magnification factor of 4.3.

source variation in the FSS was corrected by varying the potential of the focusing electrodes. The reason for adjusting FSS is to minimize the anode heat load. It is desirable to make the FSS as large as the system resolution allows. Therefore, we adjusted the FSS of all the beams to be as close to the targeted value as possible.

II.E. System modulation transfer function

Modulation transfer function (MTF) was used to characterize the ability of the imaging system to faithfully reproduce the different spatial frequencies in the imaged object. A homemade MTF phantom consists of a 100 μm diameter tungsten wire inside a Plexiglas cylinder. The wire has a 2° angle to the vertical rotation axis to allow oversampling of the line spread function.[35] The magnification factor of 1.1 was used in the measurement. The MTF phantom was put 6.5 cm from the detector. For consistency check, the detector MTF was measured by placing two cross 100 μm diameter tungsten wires directly on the surface of the detector.

II.F. Entrance exposure value distribution

In the present MBFEX source the 25 x-ray beams are arranged in a linear line parallel to the detector plane rather than along an arc. As a result, the SOD varies from beam to beam. The central x-ray beam is closer to the object than the beams from the edges. To obtain a comparable entrance exposure at the object, the x-ray flux from each beam needs to be regulated according to its respective SOD distance. This can be accomplished by modulating the corresponding x-ray tube current. Figure 5 shows the variation in the SOD and the exposure required from each x-ray beam to maintain the constant imaging exposure on the object.

II.G. X-ray intensity uniformity

X-ray intensity distribution was measured at 28 kVp, 10 m As, and 69 cm source to detector distance. No additional filter was used except the 30 μm thick Mo window. The line profiles of intensity values in the region of interest (ROI) on the detector were plotted.

II.H. Spectrum measurement

The x-ray energy spectrum was measured using an XR-100T-Si x-ray spectrum analyzer (AMPTEK, Inc., Bedford, Mass.). The detector was positioned 50 cm away from the x-ray tube.

II.I. Phantom imaging

A 3D tissue equivalent breast phantom (model 013, CIRS, Norfolk, Virginia) was employed. The phantom is shaped to represent a compressed breast, 5 cm thick. Embedded within the phantom are radiographically visible dense masses. These masses are randomly positioned. Two calcification clusters are positioned at the midplane on the right and left edges of the phantom. The phantom was placed 2.5 cm away from the detector plane. The corresponding dark and flux images under the identical conditions were also acquired.

III. RESULTS

III.A. X-ray tube current

Figure 6 shows the emission current as a function of the gate electrical field from a 2×8 mm elliptical cathode. The scanning electron microscope image of the CNT cathode is shown in Fig. 6(b). The cathode current I_{cathode} readily reached 18 mA at 12 V/μm, the highest electrical field applied in this study due to the high voltage limit of the feedthrough and the MOSFET switch. For comparison, the data from the same cathode measured in the parallel-plate geometry in the diode mode before it was assembled into the x-ray unit were plotted on the same figure. The extraction

TABLE I. Effective focal spot sizes for different CNT cathodes.

Cathodes	Effective focal spot size (mm)
2.35×0.5 mm elliptical	0.1×0.1
2×8 mm elliptical	0.5×0.3
3 mm diameter circular	0.5×0.2

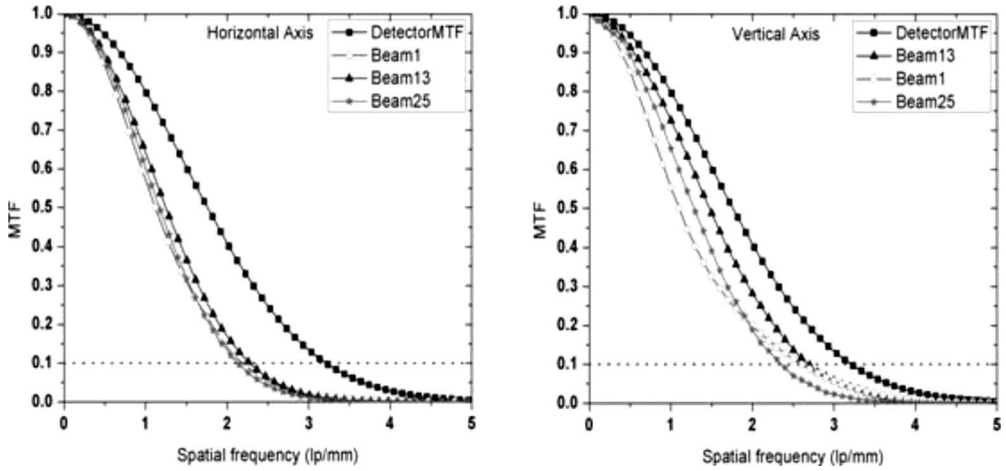

FIG. 11. The measured MTF using the homemade phantom with x-ray sources 1, 13, and 25 on, respectively. The detector MTF was measured with two cross tungsten wires on the surface of the detector with central source 13 on. 3 mm circular cathodes were used in this experiment.

field in the triode mode is higher than that in the diode mode and the curve shapes between these two modes are different. This is mainly attributed to the nonuniform electrical field created by the metal grid used as the gate electrode in the x-ray source.

The transmission rate, defined by $I_{\text{tube}}/I_{\text{cathode}}$, was calculated to be around 70%. At 18 mA cathode current, the anode current is 12.6 mA. The transmission rates for all 25 beams are shown in Fig. 7. The variation is 1.36%. The leakage currents on the gate and focusing electrodes are 30% and 0.02%, respectively, of the total cathode current.

III.B. Lifetime

Figure 8 shows a sequence of four measurements performed on the same electron source with a 2×8 mm elliptical cathode. During the measurement, the gate electrical field was automatically adjusted through a feedback loop to maintain a constant emission current. The MOSFET was triggered using the LABVIEW program developed in our laboratory. For the first three measurements shown in Fig. 8(a), the current waveform was programmed to be a square wave with 1 s pulse width. The respective duty cycles are 20% at 5 mA, 12.5% at 8 mA, and 15% at 10 mA. In the fourth measurement, the current was kept at 15 mA using 10 ms pulse width and 1% duty cycle. As shown, the cathode was found to be stable during the entire testing period. The gate voltage remained essentially stable. The total accumulated electron beam-on time for the four measurements is ~570 min.

III.C. Cathode-to-cathode consistency

To evaluate the consistency and reliability in the performance of the CNT cathodes, measurements were performed under identical conditions for 25 CNT cathodes under the parallel-plate geometry. Figure 9 shows the electrical field vs the cathode current. To reach a given emission current, such as 2 mA, the variation in the electrical field is ~1.2 V/μm (the spacer between the gate and the cathode is 200 μm). This is within the range of what can be compensated by the control electronics to deliver a constant output tube current by adjusting the applied voltage.

III.D. X-ray focal spots

The effective focal spot sizes have been measured from different size cathodes. As expected the measured result depends sensitively on the cathode dimension and the voltages applied to the two focusing electrodes, which were adjusted to obtain the minimum focal spot size. Figure 10 shows the pinhole image measured from a 3 mm diameter circular cathode using 100 μm diameter pinhole. To calculate the focal spot size using the acquired images, a ROI around the bright spot in the pinhole projection image was chosen. The intensity values within the ROI along the x and y axes were integrated and were fitted to a Gaussian function. The FSSs along the two axes were calculated using the formula FSS $=A*B/M$, where $A=1.28*c$ is the value of 80% of the area under Gaussian curve $(e^{-(x-b)^2/2c^2})$, B is the pixel pitch of the detector, and M is the magnification factor, in our case it is 4.3.

Table I shows the experimentally measured focal spot sizes from different CNT cathodes. The value for the 2.35

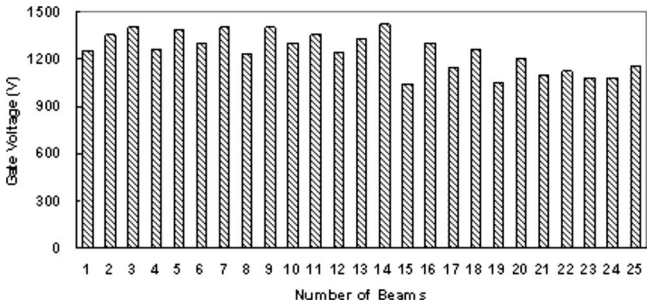

FIG. 12. Based on the SOD, the certain gate voltages are needed to obtain the constant entrance exposure of 10 m As at the object for each x-ray source. The tube current for the center beam was set at 1 mA.

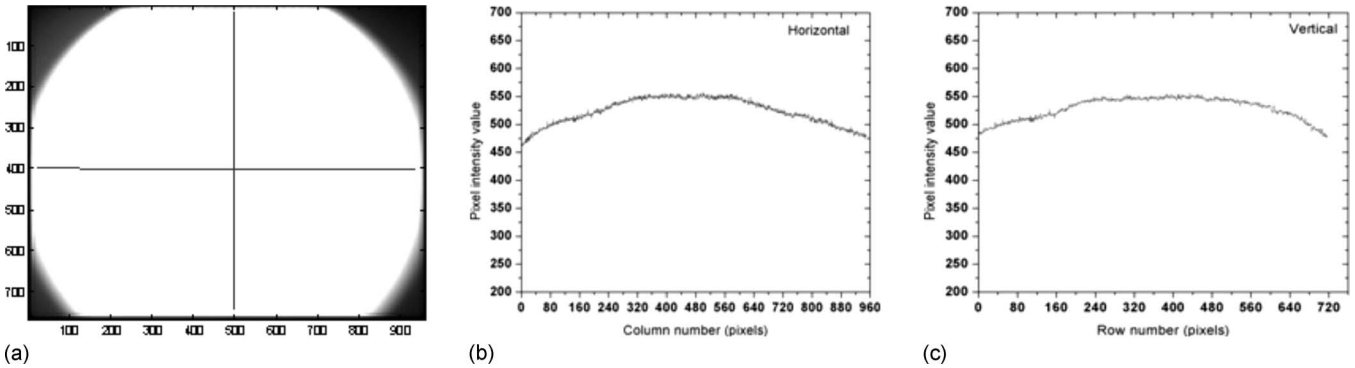

FIG. 13. (a) The x-ray intensity from the center x-ray beam recorded on the detector, (b) intensity value along the horizontal axis, and (c) intensity value along the vertical axis.

$\times 0.5$ mm^2 cathode has been reported previously.[29] The beam-to-beam variation among the 25 x-ray beams is ~ 20 μm.

III.E. Modulation transfer function

The system MTF functions associated with different x-ray beams have been measured. Figure 11 shows the experimental results from the central x-ray beam (beam 13) and the two beams from the extreme left (beam 1) and extreme right (beam 25). The spatial resolution, as measured by 10% MTF, is ~ 2.5 lines/mm in the horizontal axis and ~ 2.8 lines/mm in the vertical axis for the central beam. The MTF degrades slightly for the off-center x-ray beams. For example, for x-ray beams 1 and 25, the 10% MTF is 2.2 lines/mm in the horizontal direction and 2.5 lines/mm in the vertical direction. This is attributed to the projection angle of the x-ray beam on the detector screen. Also plotted on the same figure is the detector MTF which was measured to be 3.1 lines/mm at 10% in both directions, consistent with the reported value.[36,37]

The difference in MTFs in the two orthogonal axes is attributed to the anisotropy of the focal spot size. For the 3 mm circular cathode, the measured focal spot sizes for vertical and horizontal axes are 200 and 500 μm, respectively. Using the detector MTF of 3.1 lines/mm and the measured focal spot sizes, the spatial resolution of the system is estimated to be $0.5/(0.5/3.1+10\%*0.2)=2.8$ lines/mm for the vertical axis and $0.5/(0.5/3.1+10\%*0.5)=2.4$ lines/mm for the horizontal axis. Both agree well with the measured MTF values.

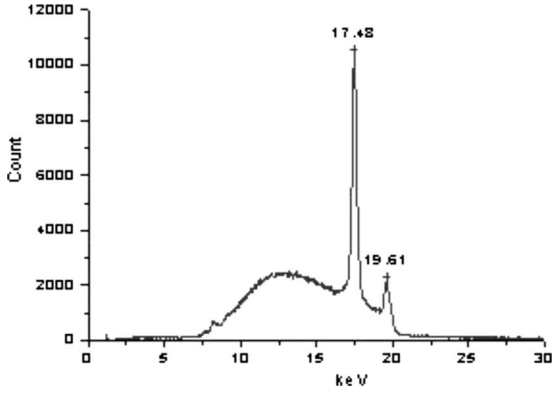

FIG. 14. The experimentally measured energy spectrum after the 30 μm thick Mo filter.

III.F. Entrance exposure value distribution

The gate voltages needed to achieve constant imaging exposure value on the object surface from the x-ray beams are shown in Fig. 12. In this experiment, the x-ray tube current for the center beam was set at 1 mA. The tube currents from the rest of the x-ray beams were set based on their SOD distances by adjusting the respective gate voltage using on the Fowler–Nordheim equation. There is no systematic trend in the actual control gate voltage from different x-ray beams due to random variations in the field emission cathodes.

III.G. X-ray intensity uniformity

Figure 13 shows the x-ray intensity recorded on the entire detector (2×2 binning) using the center x-ray beam. The x-ray intensity variations for the horizontal line are 15.1% and 13.2% in the vertical direction. The same measurement was performed for all 25 x-ray beams. The percentage variation in intensity is 13.2%–18.6% for all 25 x-ray beams. During experiments using phantoms, we mainly use the central region of 130×90 mm^2, 200–800 pixels along the x axis, and 200–600 pixels along the y axis, as shown in Fig. 12(a). Within this region, the x-ray intensity variations for the horizontal line are 5% and 4% in the vertical direction. The percentage variation in intensity is 4%–9% for all 25 x-ray beams.

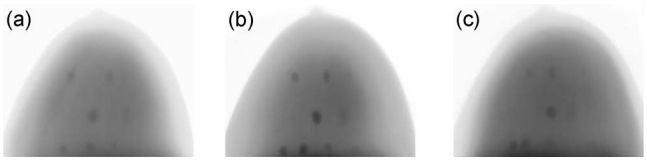

FIG. 15. Breast phantom projection images obtained by our system using three individual x-ray sources (a) x-ray source 1, (b) x-ray source 13, and (c) x-ray source 25.

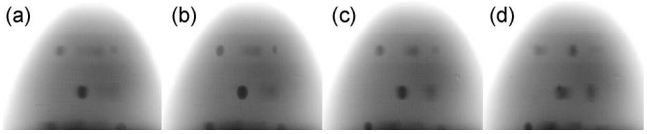

FIG. 16. Four slices of the reconstructed breast phantom image are shown here. These slices are at the depths of (a) 6 mm, (b) 11 mm, (c) 16 mm, and (d) 21 mm.

III.H. Spectrum measurement

The experimentally measured energy spectrum is shown in Fig. 14, which agrees well with typical Mo/Mo x-ray spectrum, with two molybdenum characteristic peaks at 17.5 and 19.6 keV.[38]

III.I. Breast phantom imaging

Figures 15(a)–15(c) show the projection images of the breast phantom from x-ray beams 1, 13, and 25. The images were obtained using 28 kVp, molybdenum filter, molybdenum target, and 100 m As per view. For this experiment, 3 mm diameter circular CNT cathodes were used. The masses in the phantom were visualized in all 25 views.

To perform tomosynthesis of the breast phantom, 25 projection images were obtained from the system at a total exposure of 100 m As (4 m As/beam). The same experimental condition was used: 28 kVp, molybdenum filter, and molybdenum target. These projection images were then reconstructed using the modified ordered subsets convex method and design geometry parameters to yield 60 slices through the phantom. The slice distance is 1 mm. Figure 16 shows four slices at the depths of 6, 11, 16, and 21 mm from the top of the phantom. These slices clearly demonstrate the different masses getting focused at different depths. Details on the geometry calibration and image reconstruction will be reported separately.

IV. DISCUSSIONS

The stable x-ray tube current and the focal spot size depend on the area of the CNT cathode. For the 2×8 mm elliptical cathode (0.5×0.3 mm focal spot), a stable emission of 18 mA was readily obtained at 1800 V applied gate voltage. For an imaging protocol using 100 m As per tomosynthesis scan with 25 x-ray beams, the exposure value from each x-ray beam is 4 m As, which translates to 5.7 m As per cathode using the measured transmission rate of 70% (70% of the cathode current reached the anode). Assuming that the tube operates at the cathode current of 10 mA (the actual test was performed in multiple steps with the currents ranging from 5 to 15 mA), the required exposure time is 0.57 s per cathode. The 570 min electron beam-on time measured from one cathode in the stability test translates to an x-ray source array lifetime of at least 60 000 scans. For a busy mammography clinic with ~60 patients/day, the results means that MBFEX source can be operated for at least 1000 working days at this output level. During measurement the gate voltage essentially remained the same, indicating that the CNT cathode can be operated for far longer time.

The experimentally measured focal spot sizes of the 2×8 mm elliptical and 3 mm diameter circular cathodes are comparable to that of a typical commercial mammography tube without motion blurring. The lower system MTF is attributed to the low resolution of the detector used in the study which has a resolution of 3.1 lines/mm at 10% MTF. This is to be compared to the reported value.[36,37] We estimate that a system resolution of 7 lines/mm at 10% MTF can be obtained by replacing the current detector with an amorphous selenium full-field digital detector with pixel pitch of 85 μm.

For the stationary DBT scanner, the scan time (t_{scan}) is influenced by multiple factors including the number of views (N_{view}), detector readout time (t_{readout}), integration time ($t_{\text{integration}}$), total imaging exposure value (D_{total}), and x-ray tube current (I_{tube}). If the detector frame rate is not a limiting factor, then the scan time can be calculated by $t_{\text{scan}}=N_{\text{view}}\times(t_{\text{readout}}+D_{\text{total}}/(N_{\text{view}}\times I_{\text{tube}}))$. Assuming that 100 m As is the total imaging exposure value distributed evenly over the 25 beams, the relation becomes $25\times(t_{\text{readout}}+4/I_{\text{tube}})$. The relation between the scanning time and the x-ray time current is plotted in Fig. 17 for different imaging conditions.

Using the experimentally measured current of 18 mA (tube current of 12.6 mA at 70% transmission), t_{scan} is calculated to be 11.1 s at full resolution and 8.7 s with 2×2

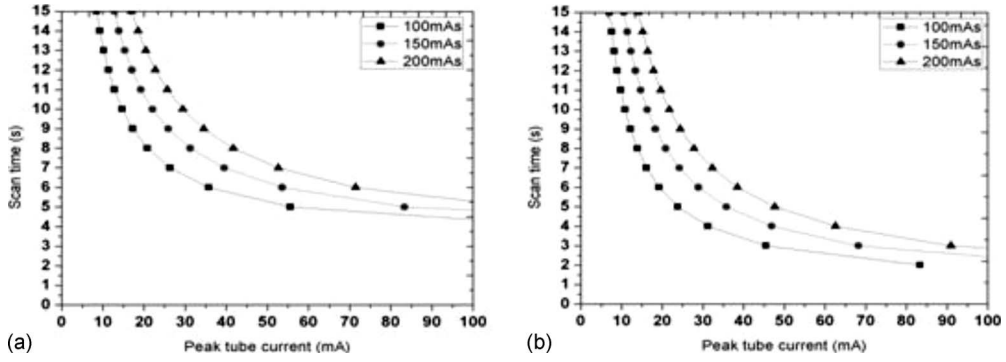

FIG. 17. The relation between the estimated scan time and the x-ray tube peak current for the cases of 100, 150, and 200 m As total imaging exposure value, respectively. (a) $t_{\text{readout}}=0.128$ s for full resolution mode. (b) $t_{\text{readout}}=0.032$ s for 2×2 binning mode.

binning for the total imaging exposure value of 100 m As without motion blurring. These values compare favorably to the reported scanning times of the prototype scanners from the commercial vendors.[10,11,13] Further reducing the scanning time can be achieved by either a detector with fast frame rate and higher tube power. For example, with the current detector, if $I_{tube}=40$ mA, then t_{scan} becomes 5.7 s at full resolution and 3.3 s with 2×2 binning. The highest cathode current measured in this study is 18 mA. This is due to limitations of the vacuum feedthrough and the MOSFET rather than the CNT cathode itself. Based on the emission stability from the current study and results from other studies, we believe that a higher current can be achieved without enlarging the cathode size and therefore the focal spot size. However, this has not been measured under the exact conditions required by this system and needs to be verified in the future. Additional factor needs to be considered with further increase in the cathode current is the anode heat load.

V. CONCLUSION

In this study, we demonstrated the feasibility of constructing a spatially distributed multibeam field emission x-ray source array for s-DBT. The technology has the potential to increase the resolution and reduce the imaging time for digital breast tomosynthesis. The flexibility in the configuration of the x-ray source array will also allow system designers to consider imaging geometries that are difficult to achieve with the conventional single-source rotating approach. With the present design of 25 views, we demonstrated experimentally the feasibility of achieving 11 s scanning time at full detector resolution with 0.5×0.3 mm source resolution without motion blur. We believe there is room to further reduce the scanning time to below 5 s with further improvement of the system. The system resolution can be improved by using a higher resolution detector.

ACKNOWLEDGMENTS

One of the authors (O.Z.) acknowledges supports from NCI (Grant No. U54CA119343) and the Lineberger Comprehensive Cancer Center and the University Cancer Research Fund at the University of North Carolina. One of the authors (X.C.) was supported by a graduate fellowship from NIBIB (Grant No. R33EB004204-S). The authors thank Dr. J. Geng and Dr. B. Gao of Xintek for technical assistance in CNT cathode fabrication and Dr. Sprenger of XinRay for discussions on x-ray focal spot measurement. They acknowledge discussions with Professor E. Pisano and Ms. E. Cole of UNC Radiology and Professor Y. Chen of SIU.

[a]Electronic mail: xqian@physics.unc.edu
[b]Electronic mail: zhou@physics.unc.edu

[1]E. D. Pisano *et al.*, "Diagnostic performance of digital versus film mammography for breast-cancer screening," N. Engl. J. Med. **353**, 1773–1783 (2005).
[2]L. W. Bassett *et al.*, *Diagnosis of Diseases of the Breast*, 2nd ed. (Elsevier Saunders, Philadelphia, PA, 2005).
[3]L. Niklason, "Digital tomosynthesis in breast imaging," Radiology **205**, 399–406 (1997).
[4]J. T. Dobbins III and D. J. Godfrey, "Digital x-ray tomosynthesis: Current state of the art and clinical potential," Phys. Med. Biol. **48**, R65–R106 (2003).
[5]T. Wu *et al.*, "Tomographic mammography using a limited number of low-dose cone-beam projection images," Med. Phys. **30**(3), 365–380 (2003).
[6]Y. Chen, J. Y. Lo, and J. T. Dobbins, "Impulse response analysis for several digital tomosynthesis mammography reconstruction algorithms," Proc. SPIE **5745**, 541–549 (2005).
[7]M. Bissonnette *et al.*, "Digital breast tomosynthesis using an amorphous selenium flat panel detector," Proc. SPIE **5745**, 529–540 (2005).
[8]Y. Zhang *et al.*, "A comparative study of limited-angle cone-beam reconstruction methods for breast tomosynthesis," Med. Phys. **33**(10), 3781–3795 (2006).
[9]A. D. Maidment *et al.*, "Evaluation of a photon-counting breast tomosynthesis imaging system," Proc. SPIE **6142**, 89–99 (2006).
[10]B. Ren *et al.*, "Design and performance of the prototype full field breast tomosynthesis system with selenium based flat panel detector," *Proceedings of SPIE Physics of Medical Imaging* (SPIE, Bellingham, WA, 2005), Vol. 5745.
[11]M. Bissonnette *et al.*, *Proceeding of SPIE Medical Imaging 2005: Physics of Medical Imaging* (SPIE, Bellingham, WA, 2005), Vol. 5745.
[12]Z. Bo *et al.*, "Experimental validation of a three-dimensional linear system model for breast tomosynthesis," *Proceedings of AAPM* (SPIE, Bellingham, WA, 2009), pp. 240–251.
[13]J. Zhou, B. Zhao, and W. Zhao, "A computer simulation platform for the optimization of a breast tomosynthesis system," Med. Phys. **34**(3), 1098–1108 (2007).
[14]S. P. Poplack *et al.*, "Digital breast tomosynthesis: Initial experience in 98 women with abnormal digital screening mammography," AJR, Am. J. Roentgenol. **189**, 616–623 (2007).
[15]G. M. Stevens *et al.*, "Circular tomosynthesis: Potential in imaging of breast and upper cervical spine: Preliminary phantom and in vitro study," Radiology **228**, 569–575 (2003).
[16]P. Baldelli *et al.*, "A prototype of a quasi-monochromatic system for mammography applications," Phys. Med. Biol. **50**, 2225–2240 (2005).
[17]P. Baldelli *et al.*, "Dose comparison between conventional and quasi-manochromatic systems for diagnostic radiology," Phys. Med. Biol. **49**, 4135–4146 (2004).
[18]D. J. Crotty, R. L. McKinley, and M. P. Tornai, "Experimental spectral measurements of heavy K-edge filtered beams for x-ray computed mammotomography," Phys. Med. Biol. **52**, 603–616 (2007).
[19]R. L. Mckinley *et al.*, "Simulation study of a quasi-monochromatic beam for x-ray computed mammotomography," Med. Phys. **31**(4), 800–813 (2004).
[20]R. A. Robb *et al.*, "High-speed three-dimensional x-ray computed tomography: The dynamic spatial reconstructor," Proc. IEEE **71**(3), 308–319 (1983).
[21]M. Petersilka *et al.*, "Technical principles of dual source CT," Eur. J. Radiol. **68**(3), 362–368 (2008).
[22]M. J. Lipton *et al.*, "Cardiac imaging with a high-speed cine-CT scanner: Preliminary results," Radiology **152**(3), 579–582 (1984).
[23]M. A. Speidel *et al.*, "scanning-beam digital x-ray (SBDX) technology for interventional and diagnostic cardiac angiography," Med. Phys. **33**(8), 2714–2727 (2006).
[24]T. G. Schmidt *et al.*, "A prototype table-top inverse-geometry volumetric CT system," Med. Phys. **33**(6), 1867–1878 (2006).
[25]J. Zhang *et al.*, "A stationary scanning x-ray source based on carbon nanotube field emitters," Appl. Phys. Lett. **86**, 184104 (2005).
[26]J. Zhang *et al.*, "A multi-beam x-ray imaging system based on carbon nanotube field emitters," *Proceedings of SPIE Medical Imaging 2006*, edited by M. J. Flynn and J. Hsieh (SPIE, Bellingham, WA, 2006), Vol. 6142, p. 614204.
[27]J. Zhang *et al.*, "Multiplexing radiography using a carbon nanotube based x-ray source," Appl. Phys. Lett. **89**, 064106 (2006).
[28]D. S. Lalush, "Binary encoding of multiplexed images in mixed noise," IEEE Trans. Med. Imaging **27**(9), 1323–1332 (2008).
[29]G. Cao *et al.*, "A dynamic micro-CT scanner based on a carbon nanotube field emission x-ray source," Phys. Med. Biol. **54**, 2323–2340 (2009).
[30]J. S. Maltz *et al.*, "Fixed gantry tomosynthesis system for radiation therapy image guidance based on a multiple source x-ray tube with carbon nanotube cathodes," Med. Phys. **36**(5), 1624–1636 (2009).

[31]G. Yang *et al.*, "Stationary digital breast tomosynthesis system with a multi-beam field emission x-ray source array," *Proceedings of SPIE Physics of Medical Imaging* (SPIE, Bellingham, WA, 2008), Vol. 6913, p. 69131A:1–10.
[32]Z. Liu *et al.*, "Carbon nanotube based microfocus field emission x-ray source for microcomputed tomography," Appl. Phys. Lett. **89**, 103111 (2006).
[33]O. Van der Biest and L. J. Vandeperre, Annu. Rev. Mater. Sci. **29**, 327–352 (1999).
[34]European Committee for Standardization, EN 12543-2, 1999 E, Brussels, 1999.
[35]E. A. Fujita, "Simple method for determining the modulation transfer function in digital radiography," IEEE Trans. Med. Imaging **11**(1), 34–39 (1992).
[36]X. Wang, Y. Han, and J. Si, "Non-uniformity emendation technique for amorphous silicon flat-panel detectors used for industrial x-ray digital radiography," Measurement **41**, 817–822 (2008).
[37]E. Samei, "Image quality in two phosphor-based flat panel digital radiographic detectors," Med. Phys. **30**(7), 1747–1757 (2003).
[38]J. Beutel *et al.*, *Handbook of Medical Imaging* (SPIE Press, Bellingham, WA, 2000).